Advances in Science and Technology Research Journal

*Advances in Science and Technology Research Journal*, 2026, 20(9), 209–223
https://doi.org/10.12913/22998624/221918
ISSN 2299-8624, License CC-BY 4.0

Received: 2026.04.22
Accepted: 2026.07.10
Published: 2026.08.01

# Experimental analysis of high-pressure water jet velocity and kinetic energy using a high-speed camera

Michał Leleń[1*], Jerzy Józwik[1]

[1] Department of Production Engineering, Lublin University of Technology, Nadbystrzycka 38D, 20-618 Lublin, Poland

* Corresponding author's e-mail: m.lelen@pollub.pl

## ABSTRACT

This study presents the results of experimental investigations into the dynamic and energetic characteristics of a high-pressure water jet using high-speed imaging in conditions relevant to abrasive water jet machining (AWJ) applications. The scientific contribution of the work lies in the combined experimental determination of jet velocity and kinetic energy over a wide operating pressure range, together with a direct comparison between measured jet characteristics and a simplified Bernoulli-based analytical model. The aim of the study was to determine jet velocity at different operating pressure levels, evaluate the corresponding kinetic energy, and compare the experimental results with theoretical values calculated using a simplified Bernoulli-based model. The experiments were carried out on an Eckert Combo machine using a Phantom V1610 high-speed camera. Measurements were performed for five operating pressure levels: 50, 100, 200, 300, and 380 MPa. The recorded video sequences were analyzed in TemaMotion software, which made it possible to determine the displacement, velocity, and acceleration histories of a characteristic point of the jet, as well as the mean values of experimental jet velocity. The experimental velocity increased from 144 m/s at 50 MPa to 430 m/s at 380 MPa, while the corresponding theoretical values ranged from 316.23 m/s to 871.78 m/s. The relative deviation between the experimental and theoretical results ranged from -39.92% to -54.46%. On this basis, the kinetic energy of the jet was determined and was found to increase from 0.00814 J to 0.07260 J for the experimental data and from 0.03927 J to 0.29845 J for the theoretical model. The obtained results indicate that operating pressure significantly affects the dynamic response and energy potential of the water jet, with the increase in kinetic energy representing the most important effect from the standpoint of its technological potential. The results also show that kinetic energy provides a more informative measure of the technological potential of the jet than velocity alone, while at the same time revealing the limitations of the idealized Bernoulli-based description under real experimental conditions. In this way, the study contributes to a more quantitative understanding of pressure-dependent jet behavior in systems relevant to AWJ applications.

**Keywords:** high-pressure water jet, water jet dynamics, high-speed imaging, jet velocity, kinetic energy, theoretical modelling.

## INTRODUCTION

High-pressure water jets and AWJ are among the most extensively studied non-conventional machining methods for difficult-to-machine materials, including composites. The strong interest in this technology arises from the high energy potential of the jet and its applicability to the machining of materials with complex structures. From the standpoint of process description, understanding jet dynamics is of particular importance, especially in terms of jet velocity, stability, and changes in energy potential as a function of supply parameters.

Previous studies on the AWJ process have focused both on the evaluation of technological outcomes and on the analysis of jet dynamics and energetics. At the same time, experimental methods enabling direct measurement of jet velocity and structure, as well as numerical models based on computational fluid dynamics (CFD), smoothed particle hydrodynamics (SPH), the finite element method (FEM), and their hybrids, have been continuously developed. Despite significant progress in the description of the AWJ process, further research is still needed on the relationship between operating pressure and the actual dynamic parameters of the jet, as well as on the possibilities of validating simplified theoretical models using optical methods [1].

In studies on high-pressure abrasive water jet cutting, particular attention has been paid to the analysis of jet interaction mechanisms and the factors affecting process efficiency. Chen and Siores [2] demonstrated that striation formation in the AWJ process is directly related to the non-uniform distribution of the kinetic energy of abrasive particles across the jet cross-section. Non-contact measurements using Laser Doppler Anemometry revealed a wave-like distribution of particle velocity and concentration, leading to local differences in interaction energy. The authors also pointed out that, with increasing depth of cut, the number of particles whose energy exceeds the material destruction threshold decreases, thereby affecting the nature of the process in the lower interaction zone of the jet.

This issue was further developed in studies concerning the dynamics of the cutting system. Monno and Ravasio [3] showed that cutting head vibrations are among the key factors influencing the formation of striations on surfaces generated in both pure water jet and abrasive water jet cutting. Based on the analysis of vibration signals and roughness spectra, they proposed a geometric model describing the dependence of the spatial period and amplitude of striations on the frequency and amplitude of jet vibrations. Validation of the model confirmed a close relationship between cutting system dynamics, jet energy distribution, and cutting surface quality.

These considerations are complemented by studies on modifications of cutting kinematics. Lemma et al. [4] compared conventional AWJ cutting and AWJ cutting with head oscillation during the machining of glass fiber-reinforced polymer (GFRP) composites, indicating that superimposed oscillatory motion may reduce striation formation in the lower cutting zone and improve kerf wall quality. A reduction in roughness *Ra* of up to approximately 20% was demonstrated for appropriately selected oscillation parameters, with the effect of oscillation angle being stronger than that of oscillation frequency.

Understanding the mechanisms responsible for surface quality requires an analysis of jet energy characteristics and the energy balance in the interaction zone. Studies on the energy balance of abrasive water jet erosion have highlighted the role of the kinetic energy of wear particles removed from the material [5]. It was shown that, despite the increase in the kinetic energy of such particles with erosion depth, their share in the total jet energy is small and amounts to about 0.3% of the AWJ input energy, indicating the possibility of simplifying energy-based models of the cutting process.

In parallel, experimental methods for analyzing water jet dynamics have also been developed. Zelenák et al. [6] presented methods for the visualization and measurement of velocity fields in continuous and pulsating water jets generated in high-pressure systems. The application of the shadowgraph technique combined with particle image velocimetry (PIV) algorithms enabled the analysis of jet geometry and velocity distribution, both of which are important from the standpoint of efficient kinetic energy transfer to the material. The authors pointed out the usefulness of these methods both for CFD model validation and for the optimization of nozzle design and process parameters.

An important complement to studies on jet development is provided by optical experiments concerning jet initiation and the early stage of its formation. Znamenskaya et al. [7] carried out detailed investigations of the dynamics of a jet generated at very high pressure using shadow imaging, a high-speed camera, and a thermographic camera. This made it possible to directly measure the velocity of the jet front and its acceleration; it was shown that the jet reaches velocities on the order of several hundred meters per second within a very short time after initiation. A similar line of research was presented by Zelenák et al. [8], who used a high-speed camera and the PIV technique to analyze the velocity fields of a self-excited water jet generated by a hydrodynamic nozzle. It was demonstrated that, with increasing operating pressure, the maximum jet velocity rises to approximately 250 m/s, while its decrease along the jet axis amounts to 13–15% within the range of 0–100 mm from the nozzle exit, providing data for flow model validation and analyses of kinetic energy transport.

An important direction in the development of AWJ research involves strategies for reducing typical surface defects, such as striations, kerf taper, and local cutting-surface damage in hybrid structures. Li et al. [9] showed that, in the case of aluminum alloy/carbon fiber-reinforced polymer (Al/CFRP) stacks, the application of a dual-pass abrasive waterjet slotting strategy can significantly reduce kerf taper and decrease the intensity of striations without substantially reducing process efficiency. The authors also reported improved kerf profile quality and a reduction in the maximum height of surface irregularities, indicating that a properly designed machining strategy can effectively compensate for the decrease in the erosive capability of the jet with increasing cutting depth.

Experimental findings are directly reflected in the development of numerical modeling of the AWJ process. More recent studies have combined experiments with advanced simulations in order to quantitatively assess the influence of abrasive water jet parameters on the material removal mechanism and the scale of damage in composites [10,11]. The use of a coupled FEM–SPH model made it possible to reproduce the interactions between water, abrasive particles, and the workpiece material, including grain fragmentation phenomena and the distribution of kinetic energy within the jet interaction zone [10].

A linear relationship was demonstrated between cutting depth and operating pressure, along with a significant influence of feed rate and impact angle on kerf geometry and surface quality. Numerical investigations are complemented by recent experimental studies on the machining of fiber-reinforced polymer composites, which have shown that appropriate selection of water pressure, feed rate, and abrasive flow rate can reduce surface roughness and decrease the kerf taper angle, while the presence of carbon fibers may additionally improve dimensional stability and post-machining surface integrity in the AWJ process [12].

A further development of research on jet–material interaction is represented by studies devoted to the characterization of phenomena accompanying the AWJ machining of composite materials. Hejjaji et al. [13] demonstrated that the surfaces of carbon/epoxy composites machined by abrasive water jet may exhibit craters, material ridges, fractured fibers, and embedded abrasive particles, and that the intensity of these effects increases with jet pressure. These findings confirm that the dynamic and energetic parameters of the jet directly affect the nature of its interaction with the material, thereby justifying the need for their quantitative analysis.

In the context of predictive reliability, the need for simultaneous modeling of jet flow and material erosion has been emphasized. Guo et al. showed that reliable representation of the abrasive water jet cutting process requires coupling SPH and FEM methods and determining the actual outlet particle velocities based on CFD analyses [14]. The resulting relationships between cutting depth, pressure, and feed rate showed good agreement with experimental results. To reduce computational cost while preserving the ability to reproduce multiphase phenomena, Yu et al. developed an unresolved coupled smoothed particle hydrodynamics–discrete element method (SPH–DEM) model that enables the description of kinetic energy dissipation and erosion mechanisms in ductile and brittle materials [15].

Numerical validation procedures also play an important role. Zaki et al. presented a validation procedure for AWJ process simulation based on coupling a CFD solver with a simplified material erosion model [16]. It was shown that accurate representation of the free jet, the impact phenomenon, and abrasive particle transport is a prerequisite for further modeling of material removal. These studies were further developed in the work of Wang et al., who demonstrated that the application of the SPH method combined with classical FEM makes it possible to overcome problems associated with large deformations and mesh instability, enabling quantitative prediction of cutting depth with good agreement with experiment [17]. In turn, Özcan et al. proposed an analytical, calibration-free model for predicting cutting depth and kerf profile in controlled-depth abrasive water jet machining, based on the kinetic energy balance of abrasive particles and the machinability number of the material, with shape simulation using a signed distance field (SDF) [18].

At the same time, research has also been directed toward reducing interlaminar damage in CFRP composites, particularly during piercing and cutting initiation in abrasive water jet machining. In the context of delamination, a process modification involving the early introduction of abrasive particles into the jet, already at the stage of its formation, has been proposed [19]. As shown by Popan et al., obtaining a homogeneous AWJ stream during the initial phase of interaction with the material makes it possible to reduce the shock wave responsible for the initiation of delamination, while the response surface methodology (RSM) analysis indicated the importance of synchronizing abrasive feed, low operating pressure, and a short nozzle stand-off distance.

Technological studies are complemented by approaches based on intelligent methods. Vundavilli et al. [20] proposed a fuzzy logic-based expert system for predicting cutting depth in the AWJ process (pressure, nozzle diameter, abrasive flow rate, and feed rate), demonstrating improved accuracy after optimization of the rule base using a genetic algorithm. The application of artificial intelligence methods to reduce delamination was also presented in studies on CFRP piercing, where artificial neural network (ANN) models captured nonlinear relationships between process parameters (including water pressure, nozzle stand-off distance, and abrasive feed synchronization) and the size of the damage zone [21].

An important practical aspect is the evaluation of the influence of basic technological parameters on the energy potential of the jet and the quality of the cut surface. Spadło and Krajcarz presented a synthetic analysis of AWJ process parameters, indicating that increasing operating pressure and appropriate selection of abrasive flow rate increase the kinetic energy of the jet, which translates into greater cutting depth and lower roughness, whereas excessive feed rate promotes jet lag and deterioration of quality in the lower cutting zone [22]. In studies on kerf characteristics and cross-sectional quality in CFRP laminates cut by abrasive water jet with steel slag abrasive, Qian et al. [23] showed that the cut cross-section includes a typical initial damage zone, an erosion wear zone, and a striation zone, while fiber delamination and matrix chipping may occur on the surface; at the same time, the proposed abrasive material may represent a cost-effective alternative to garnet while maintaining comparable cutting capability.

In diagnostic studies, Perec, Kawecka, and Zając proposed the use of the footprint angle as an indicator of AWJ cutting quality and efficiency, strongly correlated with cutting depth and surface roughness, which may support adaptive process control [24]. The issue of energy concentration in the interaction zone was also analyzed by Ning et al., who investigated coating removal by means of a high-pressure water microjet; a dominant effect of total exposure time and the existence of a stagnation zone governing damage initiation were demonstrated and confirmed by CFD simulations [25].

In summary, the literature review by Karataş and Gökkaya [26] indicates that the limitations of conventional methods in the machining of CFRP/GFRP materials constitute a strong motivation for the development of non-conventional techniques, including AWJ. At the same time, the need for further research on jet energetics, process stability, and the mechanisms of interlaminar damage initiation, particularly in the context of structural applications, was emphasized.

An analysis of the available studies indicates that high-pressure abrasive water jet cutting is a multifactorial process in which cut surface quality and the scale of interlaminar damage are related to the distribution of jet kinetic energy, its stability, and the dynamics of the cutting system [2,3]. It has been shown that striation formation and deterioration of quality in the lower cutting zone result from both the energetic nonuniformity of the jet and cutting head vibrations as well as changes in process kinematics [2,4]. Optical methods (high-speed imaging, PIV, and shadowgraphy) have provided data on jet velocity and structure [6,8], while the development of CFD/SPH/FEM models has enabled increasingly accurate reproduction of phase interactions and erosion mechanisms [10,18]. At the same time, the literature indicates that the quantitative prediction of jet behavior and its energy potential under real flow conditions remains a significant challenge, particularly with regard to the initial stage of jet formation and propagation [19,21].

Based on the literature review, the following research gaps can be identified:

- a limited number of studies combining direct jet velocity measurements obtained using a high-speed camera with a quantitative analysis of jet energy potential,
- insufficient understanding of the effect of operating pressure on water jet dynamics under conditions close to those encountered in the actual AWJ process,
- limited availability of experimental data that could provide a basis for validating models describing jet development and energy transfer in abrasive water jet cutting, and
- a lack of a consistent link between the dynamic parameters of the jet and the evaluation of its suitability for analyzing process efficiency.

The aim of the present study is an experimental analysis of the velocity and kinetic energy of a high-pressure water jet in the context of the AWJ process, using a high-speed camera for the registration of rapidly changing phenomena. The study includes direct measurements of jet dynamics for different operating pressure values, determination of the corresponding experimental jet velocity values, and evaluation of jet kinetic energy for a selected elementary segment. An additional objective is to compare the experimental results with a simplified theoretical model and to determine the relationship between operating pressure and the dynamic parameters of the jet. The obtained results are expected to contribute to a better understanding of the phenomena accompanying jet formation and propagation and to provide a basis for further validation of models describing jet development, its dynamics, and its energy potential in the AWJ process.

## MATERIALS AND METHODS

### Experimental setup and test conditions

In the present study, the recorded and analyzed object was the high-pressure water jet generated by the system; the measurements focused on jet propagation between the nozzle outlet and the water surface under repeatable laboratory conditions relevant to AWJ applications. The test setup was extended by a rapid-event recording system based on a Phantom V1610 high-speed camera. A view of the experimental setup used in the study is shown in Figure 1.

The aim of the study was to analyze the velocity of the water jet generated at different operating pressure values and to determine the corresponding kinetic energy. Measurements were performed for five pressure levels: 50, 100, 200, 300, and 380 MPa. For each pressure value, five independent measurement repetitions were carried out to ensure the reliability of the results and to enable statistical analysis. The nozzle diameter remained constant throughout the entire test range, which made it possible to eliminate the influence of outlet geometry variations on jet characteristics.

The measurement section length was defined as the distance from the nozzle outlet to the water surface. This section corresponded to the actual stand-off distance occurring during the material cutting process, which allowed the obtained results to be directly related to technological conditions. The experiments were conducted at an ambient temperature of 21 °C. Temperature fluctuations during the tests did not exceed ±0.5° C, which minimized the effect of changes in the physical properties of water on the measurement results. A nozzle with a


**Figure 1.** Experimental setup used in the study, including the Eckert Combo abrasive water jet cutting machine and the rapid-event recording system with a high-speed camera Phantom V1610 and lighting system

diameter of $d$ = 1.0 mm was used in the experiments. The length of the analyzed measurement section, corresponding to the distance from the nozzle outlet to the water surface, was 200 mm. This distance was kept constant for all measurement variants. To ensure the comparability of the results, the system geometry, camera position, and lighting configuration were not changed during the measurement series.

### Image acquisition system

Water jet recording was carried out using a Phantom V1610 high-speed camera. The recordings were acquired at a resolution of 1280 × 800 pixels and a frame rate of 50,000 fps, which provided sufficient temporal resolution for analyzing jet motion at high velocities. A short exposure time was used to minimize motion blur. The field of view of the optical system covered the entire analyzed measurement section as well as the reference markers used for spatial calibration. The recordings were performed with the camera maintained in a fixed position relative to the jet axis, which reduced the effect of perspective changes on the measurement results. All video sequences were acquired using identical imaging parameters throughout the entire experimental series.

The camera was equipped with a Nikon ED AF NIKKOR 80–200 mm f/2.8D lens, which provided adequate magnification of the analyzed area. Illumination of the test stand was provided by one HEDLER HF65 lamp and two DEDOCOOL lamps mounted on MANFROTTO 1178 tripods. The applied lighting system enabled unambiguous identification of both the jet boundaries and the reference markers.

The exposure time and the recording window were kept constant for all tested pressure variants in order to ensure the comparability of the recorded image sequences. The adopted imaging configuration was selected to provide sufficient temporal resolution for tracking the jet front and to minimize motion blur during the analysis.

The main parameters of the recording system included a throughput of 16 Gpx/s, a maximum resolution of 1280 × 800 px, a recording rate of 50 000 fps at full resolution, a maximum recording speed of 1,000,000 fps at a resolution of 128 × 16 px, ISO sensitivity of 38,000T for the monochrome sensor and 3500T for the color sensor, a 12-bit bit depth, a pixel size of 28 μm, and a minimum exposure time of 1 μs.

### Jet velocity determination procedure

Reference points were placed within the measurement zone, including fixed markers and a dynamic point moving along the jet axis toward its terminal section. The entire measurement area, together with the markers, was located within the camera field of view, which made it possible to simultaneously record the system geometry and the motion of the water jet.

The recorded video sequences were analyzed using TemaMotion software, designed for object motion tracking based on high-speed image sequences. Spatial calibration was performed using the known geometry of the reference markers placed within the measurement area, which enabled image coordinates to be converted into actual displacement values. An example screenshot from TemaMotion is shown in Figure 2. The spacing between the reference markers was 10 mm, and calibration was carried out separately for each measurement series before the analysis of the image sequences began.

Jet velocity was determined by tracking the motion of a characteristic point corresponding to the jet front in successive frames of the recorded sequence. On this basis, the displacement of the point was determined as a function of time, and the instantaneous velocity was then calculated according to Equation 1.

$$v = \frac{\Delta x}{\Delta t} \tag{1}$$

where: $v$ – instantaneous jet velocity,
$\Delta x$ – displacement of the analyzed point,
$\Delta t$ – time interval between successive image frames.

For each operating pressure value, five independent measurement repetitions were performed. For each repetition, the maximum jet-front velocity was identified from the recorded velocity history. The reported experimental velocity for a given pressure level was then determined as the mean value of the maximum velocity obtained from the five repetitions, and the corresponding standard deviation was used in the graphical presentation. The experimental values determined in this way formed the basis for further comparative analysis and were used to calculate the kinetic energy of the water jet.

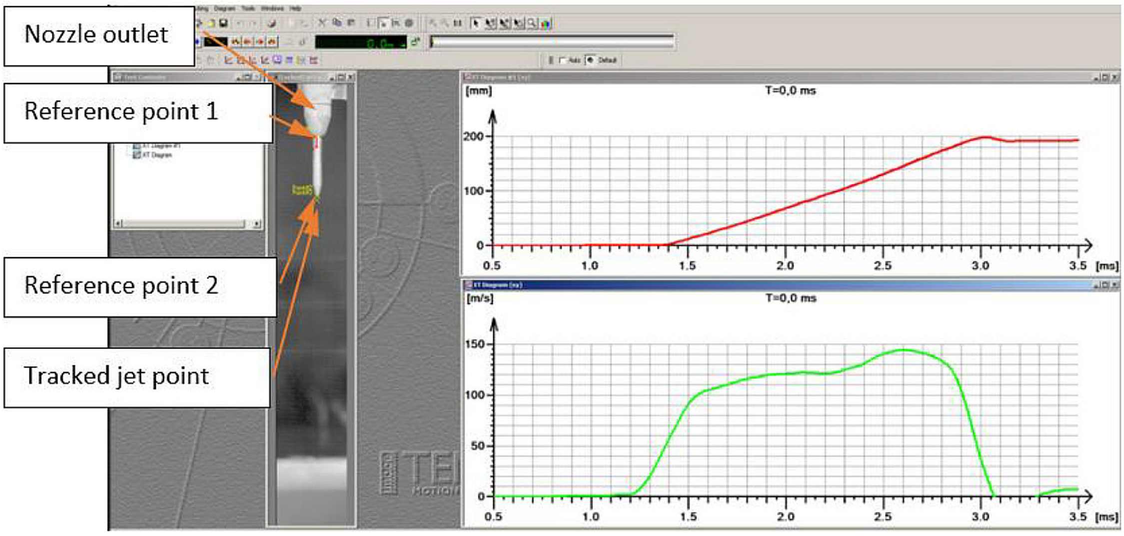


**Figure 2.** Screenshot from TemaMotion used for the analysis of water jet video sequences
**Note:** The left panel shows the measurement area with the nozzle outlet, reference points, and the tracked jet point, whereas the right panel presents the corresponding displacement history x(t) and instantane ous velocity history v(t) determined for the analyzed point

## Theoretical model of jet velocity and kinetic energy

To compare the experimental results with a simplified analytical model, theoretical values of water jet velocity and the corresponding kinetic energy were determined. The theoretical jet velocity was calculated on the basis of Bernoulli's equation, assuming ideal fluid flow and neglecting energy losses in the system, as expressed by Equation 2. It should be noted that this simplified Bernoulli-based model has a purely reference character and was used to describe the ideal pressure–velocity relationship only. The model does not account for hydraulic losses, nozzle-flow disturbances, jet contraction, turbulence, jet breakup, or interaction of the jet with the surrounding medium. Therefore, it should not be treated as a quantitatively accurate representation of the real outflow conditions, but rather as an analytical baseline for comparison with the experimental results.

$$v_{th} = \sqrt{\frac{2p}{\rho}} \tag{2}$$

where: $v_{th}$ – theoretical water jet velocity,
$p$ – water operating pressure,
$\rho$ – water density.

Based on the determined velocity values, the kinetic energy of the jet was calculated using the classical relationship given in Equation 3.

$$E_k = \frac{1}{2}mv^2 \tag{3}$$

where: $E_{k,\,th}$ – jet kinetic energy, $m$ – mass of the analyzed portion of the jet, $v$ – jet velocity.

For the calculations, an elementary jet segment with a length of $l$ = 1 mm and a diameter of $d$ = 1 mm was assumed. The adopted elementary jet segment had a reference character and was used for the comparative assessment of changes in energy potential as a function of operating pressure. The mass of the analyzed jet segment was determined from its volume and the density of water according to Equations 4–7.

$$m = \rho V \tag{4}$$

$$V = Al \tag{5}$$

The cross-sectional area of the jet was determined from the following equation:

$$A = \frac{\pi d^2}{4} \tag{6}$$

Substitution yields the following relationship:

$$m = \rho \frac{\pi d^2}{4} l \tag{7}$$

The following values were assumed in the calculations: $\rho$ = 1000 kg/m³, $d$ = 0.001 m, $l$ = 0.001 m.

After substituting the numerical values into Equation 7, the analyzed elementary jet segment was obtained as: m = 7.854 · $10^{-7}$ kg.

The mass determined in this manner was assumed to be constant for all analyzed operating pressure variants, which made it possible to directly compare changes in kinetic energy resulting from changes in jet velocity. Depending on the adopted analysis variant, the theoretical and experimental kinetic energy values were determined according to Equations 8 and 9, respectively.

$$E_{k,th} = \frac{1}{2} m v_{th}^2 \quad (8)$$

and

$$E_{k,exp} = \frac{1}{2} m v_{exp}^2 \quad (9)$$

where: $E_{k,th}$ – theoretical jet kinetic energy, $E_{k,exp}$ – kinetic energy calculated on the basis of the experimental velocity, $v_{exp}$ – velocity determined from measurements using the high-speed camera.

To compare the experimental and theoretical results, the relative velocity deviation was determined according to Equation 10.

$$\varepsilon_v = \frac{|v_{exp} - v_{th}|}{v_{th}} \cdot 100\% \quad (10)$$

With a constant nozzle outlet geometry and unchanged analysis conditions, the mass of the considered jet segment remained constant; therefore, the observed changes in kinetic energy resulted primarily from changes in jet velocity.

## RESULTS

### Qualitative analysis of water jet development

Based on the recorded video sequences obtained for individual operating pressure values, characteristic frames representing successive stages of water jet development were identified. For each test, three representative positions of the jet front were analyzed: (I) the moment of jet discharge from the nozzle, (II) the propagation phase in the section of the measurement length, and (III) the stage of jet interaction with the water surface. A set of representative frames is presented in Figure 3.

The analysis of successive stages of jet propagation is of considerable cognitive and methodological importance. In the initial stage, immediately after discharge from the nozzle, it was possible to assess the conditions of compact jet core formation and to identify potential instabilities in the outlet region. In the middle part of the measurement section, the degree of continuity and coherence of the jet was observed, which was of direct importance for determining its velocity and for evaluating its ability to maintain energy potential over a given flow path. In turn, in the zone of impact on the water surface, the character of the final interaction was analyzed,

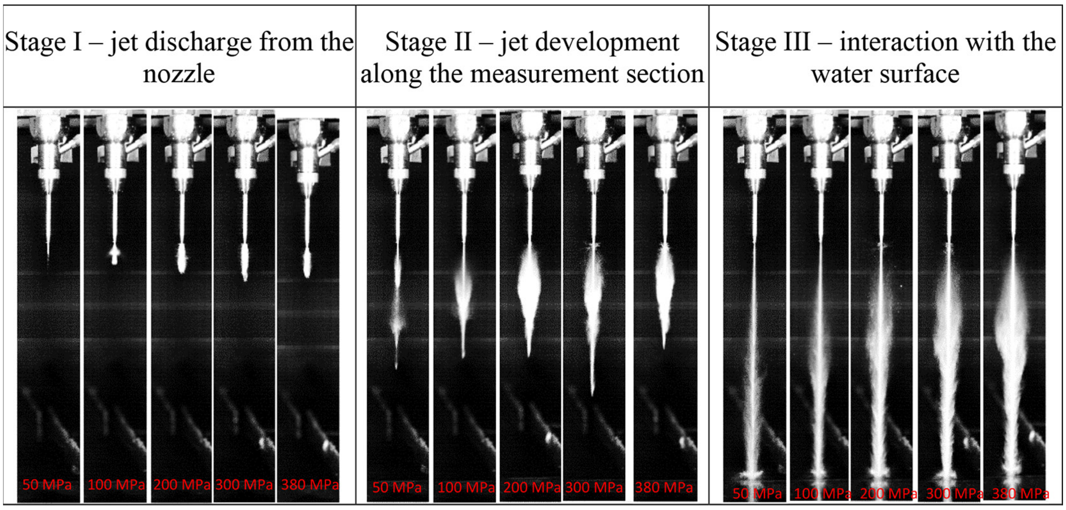


**Figure 3.** Representative frames extracted from the high-speed camera recordings, showing water jet development for five operating pressure levels: 50, 100, 200, 300, and 380 MPa. For each pressure value, three characteristic stages of jet propagation are shown: immediately after nozzle discharge, in the middle part of the measurement section, and in the jet–water surface interaction zone

including the extent of dispersion, local jet widening, and the intensity of phenomena accompanying the impact, which indirectly reflect the level of retained momentum and kinetic energy.

Based on visual observations, it was found that increasing operating pressure affected the mode of jet development over the entire measurement section. At higher pressure values, more intensive jet interaction was observed in the central zone and near the liquid surface, accompanied by an increase in the length of the effectively developed jet region and a more pronounced interaction zone after impact on the water surface. At the same time, the nature of jet dispersion changed, indicating differences in momentum transport and energy dissipation depending on the supply parameters.

## Comparison of experimental and theoretical jet velocity

In the next stage of the analysis, the experimental velocity values determined from high-speed camera recordings and data processing in TemaMotion were compared with the theoretical values calculated using the Bernoulli-based model described by Equation 2. For further analysis, experimental jet velocity values obtained at five operating pressure levels – 50, 100, 200, 300, and 380 MPa – were adopted.

To facilitate the interpretation of the recorded time histories, characteristic points and time intervals were identified on the exemplary position, velocity, and acceleration plots obtained for an operating pressure of 50 MPa, as shown in Figures 4–6.The marked points correspond to the main stages of jet development within the analyzed measurement section, whereas the highlighted intervals represent successive phases of the process observed in the adopted time window.

Based on the exemplary plots shown in Figures 4–6, five characteristic time intervals were distinguished. Interval I corresponds to the pre-initiation stage, in which the analyzed point remained stationary and the recorded values of position and velocity were close to zero. Interval II represents jet initiation and the stage of intensive acceleration, beginning at approximately t ≈ 1.2 ms, when the first distinct increase in motion of the analyzed point was observed. Within this stage, point P3 marks the end of the most intensive acceleration phase and the transition to further jet development.

Interval III corresponds to the developed propagation of the jet in the measurement section. In this range, the velocity remained high and relatively stable, while the position increased continuously. Point P5, located at approximately t = 2.5 ms, corresponds to the maximum experimental velocity of the jet. Interval IV represents the final interaction stage, in which a rapid decrease in velocity was observed, accompanied by a pronounced negative acceleration peak at point P6. This phase reflects the onset of final deceleration and the loss of jet momentum near the end of the measurement section.

Interval V corresponds to the residual stabilization stage. In this range, the position reached a plateau at approximately x = 195 mm, while the velocity remained close to zero, indicating the end of active jet motion in the analyzed time window. Point P7 marks the cessation of active motion in the measurement section, whereas point P8 denotes the end of the adopted observation window.

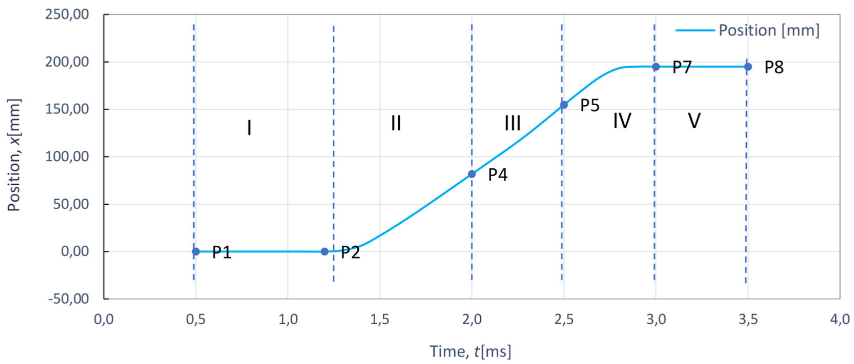


**Figure 4.** Position *x(t)* of the characteristic point of the water jet as a function of time for an operating pressure of 50 MPa, with marked characteristic points and main time intervals corresponding to successive stages of jet development

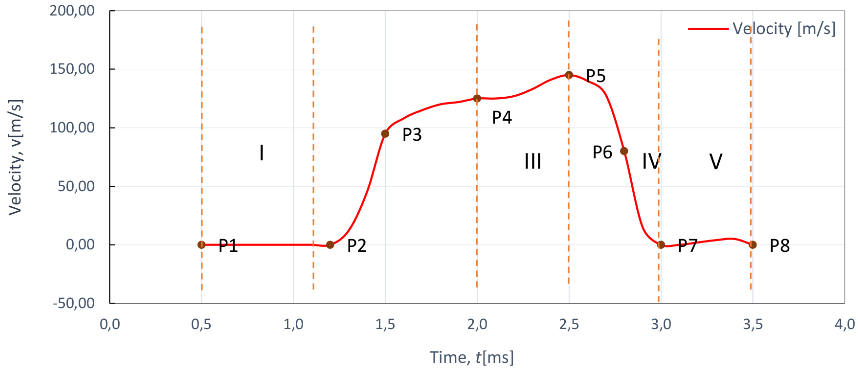


**Figure 5.** Velocity v(t) of the characteristic point of the water jet as a function of time for an operating pressure of 50 MPa, with marked characteristic points and main time intervals corresponding to successive stages of jet propagation and decay

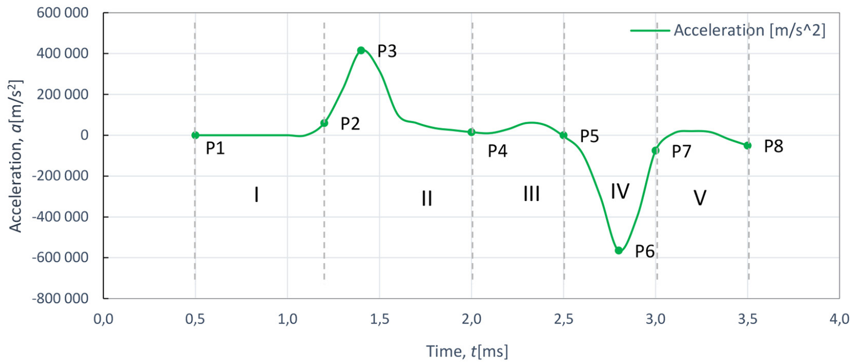


**Figure 6.** Acceleration a(t) of the characteristic point of the water jet as a function of time for an operating pressure of 50 MPa, with marked characteristic points and main time intervals used for the qualitative identification of the onset, development, and decay of jet motion

It should be emphasized that the acceleration plot was used primarily as an auxiliary and illustrative representation of the temporal evolution of the process. In the present study, the key quantitative parameter remained jet velocity, whereas the acceleration history was treated as supporting information helpful in identifying the moments of rapid onset and rapid decay of jet motion.

For a pressure of 50 MPa, the maximum experimental jet velocity determined from the recorded histories was 144 m/s, and this value was adopted for further calculations and comparison with the theoretical model.

Table 1 summarizes the operating pressure values, the experimental and theoretical jet velocities, the relative deviation between them, the corresponding experimental and theoretical kinetic energy values, and the estimated maximum acceleration of the water jet. The acceleration values should be treated as approximate comparative indicators. This combined presentation makes it possible to assess the influence of operating pressure on jet dynamics and energy potential, as well as to compare the analytical predictions with the experimentally observed behavior of the jet.

The data summarized in Table 1 show that both the experimental and theoretical jet velocities increased with operating pressure, and the same tendency was observed for kinetic energy. Throughout the entire analyzed range, the experimental values remained lower than the theoretical ones, indicating that the simplified Bernoulli-based model reproduced the general trend but overestimated the actual jet dynamics. The relative deviation ranged from -39.92% to -54.46%. Because kinetic energy depends on the square of velocity, the discrepancy between the experimental and theoretical characteristics became even more pronounced when expressed in energetic terms. The estimated maximum acceleration also increased with pressure; however, these values should be treated only as approximate comparative indicators, especially for pressure levels above 50 MPa.

**Table 1.** Comparison of experimental and theoretical jet velocity, relative deviation, kinetic energy, and estimated maximum acceleration for the analyzed operating pressure values

| Pressure [MPa] | Experimental velocity $v_{exp}$ [m/s] | Theoretical velocity $v_{th}$ [m/s] | Relative deviation [%] | Experimental kinetic Energy $E_{k,exp}$ [J] | Theoretical kinetic Energy $E_{k,th}$ [J] | Estimated maximum acceleration $a_{max}$[m/s²] |
|---|---|---|---|---|---|---|
| 50 | 144 | 316.23 | -54.46 | 0.00814 | 0.03927 | $4.15 \times 10^5$ |
| 100 | 230 | 447.21 | -48.57 | 0.02077 | 0.07854 | $6.63 \times 10^5$ |
| 200 | 380 | 632.46 | -39.92 | 0.05671 | 0.15708 | $1.10 \times 10^6$ |
| 300 | 390 | 774.60 | -49.65 | 0.05973 | 0.23562 | $1.12 \times 10^6$ |
| 380 | 430 | 871.78 | -50.68 | 0.07260 | 0.29845 | $1.24 \times 10^6$ |

To complement the tabulated results, the relationships between operating pressure and the main dynamic and energetic parameters of the water jet were additionally presented in graphical form. Figures 7–9 show the changes in experimental and theoretical velocity, kinetic energy, and estimated maximum acceleration as a function of operating pressure. This form of presentation makes it possible to identify the general tendency of change more clearly and to assess the agreement between the experimental data and the adopted analytical description.

As shown in Figure 7, both the experimental and theoretical jet velocity increased with increasing operating pressure. The experimental values followed an increasing nonlinear trend and were approximated by a second-order polynomial. At the same time, the theoretical values remained consistently higher than the experimental ones throughout the entire analyzed range. This confirms that the simplified Bernoulli-based model correctly reproduces the general tendency of velocity growth, but overestimates the actual values obtained under real experimental conditions. It should also be noted that the increase in the experimental velocity between 200 and 300 MPa was relatively small compared with the overall trend, which suggests that the local response of the measured jet front may be influenced not only by pressure itself, but also by flow instability and the limitations of optical tracking under real experimental conditions.

Figure 8 presents the relationship between operating pressure and the kinetic energy of the water jet, determined on the basis of experimental and theoretical velocity values. From the standpoint of the present study, this relationship is of particular importance, since kinetic energy constitutes the key parameter describing the energetic potential of the jet. The results clearly show that the kinetic energy increased with increasing pressure for both data series; however, the experimentally determined values remained significantly lower than the theoretical ones. This difference results directly from the lower experimental velocity values, and because kinetic energy is proportional to the square of velocity, even moderate discrepancies in velocity lead to distinctly larger differences in energy.

The plotted trend confirms that increasing operating pressure leads to a substantial increase

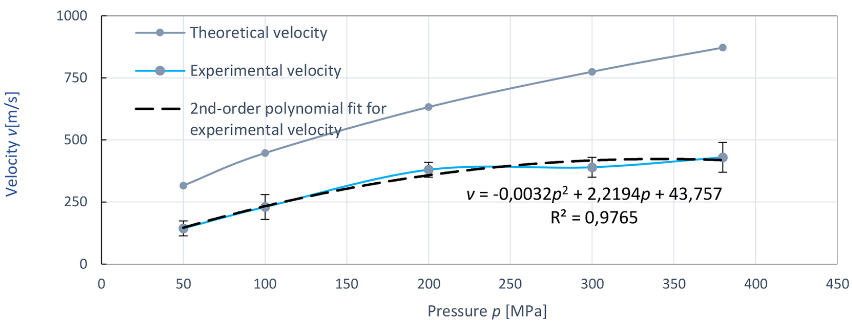


**Figure 7.** Experimental and theoretical water jet velocity as a function of operating pressure, together with the second-order polynomial fit for the experimental data. Error bars indicate the standard deviation obtained from five measurement repetitions

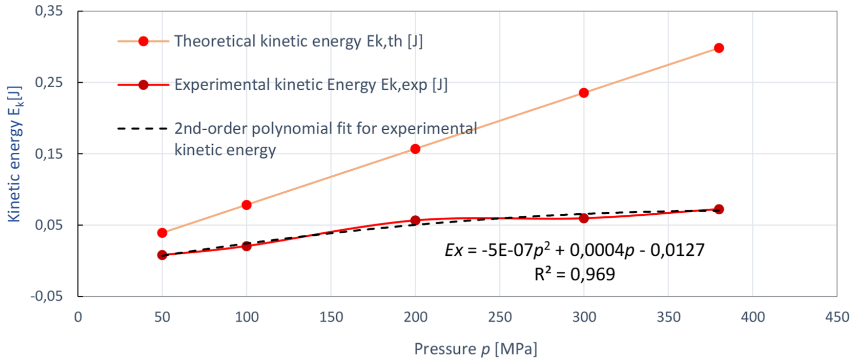


**Figure 8.** Experimental and theoretical kinetic energy of the water jet as a function of operating pressure; the fitted trendline is shown for the experimental data

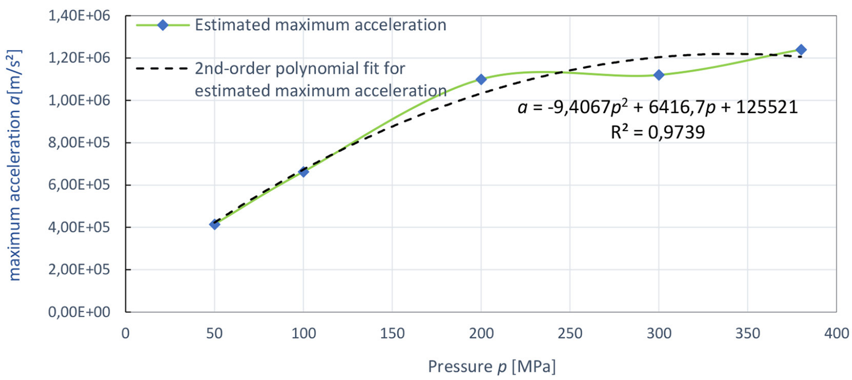


**Figure 9.** Estimated maximum acceleration of the water jet as a function of operating pressure, together with the second-order polynomial fit. The values above 50 MPa were estimated on a comparative basis and should not be interpreted as directly measured quantities

in the energetic potential of the jet. In the analyzed range, the experimental kinetic energy increased from 0.00814 J at 50 MPa to 0.07260 J at 380 MPa, whereas the theoretical kinetic energy increased from 0.03927 J to 0.29845 J. This indicates that pressure is a dominant factor governing the energy available in the jet and, consequently, its potential effectiveness in the AWJ process.

The relationship between operating pressure and the estimated maximum acceleration of the water jet is shown in Figure 9. The plotted values indicate an increasing tendency, which is consistent with the more intense dynamic response of the jet observed at higher pressure levels. It should be emphasized, however, that the acceleration values above 50 MPa were estimated proportionally on the basis of the derivative of the velocity history, using the 50 MPa case as the reference condition. Therefore, they should be interpreted as approximate comparative indicators rather than directly measured quantities for all analyzed variants.

The obtained results confirm that operating pressure is the main factor governing the dynamic and energetic characteristics of the analyzed high-pressure water jet. Both the experimental velocity and the corresponding kinetic energy increased with pressure; however, the increase in kinetic energy provides a more informative basis for interpretation, because it reflects the energetic capacity of the jet more directly than velocity alone.

A clear discrepancy was observed between the experimental and theoretical characteristics over the entire analyzed pressure range. Although the simplified Bernoulli-based model correctly reproduced the general increasing trend, it consistently overestimated the actual jet velocity. This difference became even more pronounced when expressed in terms of kinetic energy, since the error in velocity is amplified by the quadratic form of the energy relationship. This indicates that the analytical model is useful as a reference description of the pressure-dependent trend, but it is insufficient for accurate quantitative representation of the real jet without accounting for hydraulic losses, outlet-flow disturbances, and interaction with the surrounding medium. In particular, the discrepancy between the model and the experiment reflects the fact that the real jet develops under non-ideal flow conditions, which cannot be represented by a loss-free Bernoulli formulation.

The comparison of Figures 7 and 8 shows that the energetic consequences of pressure increase are more clearly revealed in the kinetic energy characteristic than in the velocity characteristic alone. In this sense, kinetic energy may be treated as a synthetic parameter that better captures the technological significance of the observed jet behavior. The qualitative observations from the high-speed recordings are consistent with this interpretation: increasing pressure was accompanied by more intensive jet propagation, greater coherence within the analyzed section, and a stronger final interaction with the water surface, which reflects the higher dynamic and energetic state of the jet.

From the point of view of AWJ machining, the obtained results indicate that pressure increase should be interpreted not only as a factor increasing jet velocity, but above all as a factor significantly increasing the energetic potential available in the interaction zone. This is important for technological interpretation, because in real machining conditions the ability of the jet to perform effective material removal depends on the energy transferred to the workpiece rather than on velocity alone. Therefore, the present results support the view that kinetic energy may serve as a more useful parameter for comparing process conditions, evaluating the potential effectiveness of the jet, and interpreting pressure-related changes in machining capability under AWJ-relevant conditions.

The acceleration characteristic shown in Figure 9 should be interpreted only as a supplementary indicator of the increasing dynamic intensity of the phenomenon. Although its trend is consistent with the observed pressure effect, the estimated character of the acceleration values above 50 MPa means that this parameter cannot be treated as a primary basis for quantitative assessment.

It should also be emphasized that the present study concerned the behavior of a high-pressure water jet in a controlled measurement section and did not include direct interaction with a machined workpiece. Therefore, the obtained results should be interpreted primarily as a basis for further analysis of jet development and energy transfer under conditions relevant to AWJ applications, rather than as a direct measure of cutting performance.

The applied approach, combining high-speed imaging, digital motion tracking, and a simplified analytical model, made it possible to identify both the actual jet response and the limitations of the idealized theoretical description. From this perspective, the study provides a useful basis for further development of energy-based descriptions of water-jet behavior in machining-related conditions.

## CONCLUSIONS

Based on the conducted investigations, the following conclusions were formulated:

1. The study provided a combined experimental assessment of water jet velocity and kinetic energy over a wide operating pressure range (50–380 MPa), which constitutes the main scientific contribution of the work in the context of pressure-dependent jet characterization under AWJ-relevant conditions.
2. The kinetic energy determined from the experimental data increased from 0.00814 J at 50 MPa to 0.07260 J at 380 MPa, which corresponds to an almost ninefold increase in the jet energy potential within the investigated pressure range.
3. The discrepancy between the theoretical and experimental characteristics remained significant throughout the entire analyzed range. While the Bernoulli-based model reproduced the overall increasing trend, it overestimated the actual jet velocity by approximately 40–55%, which resulted in an even stronger overestimation of kinetic energy.
4. The results indicate that kinetic energy is a more representative parameter than velocity alone for describing the technological potential of the jet, because it captures the energetic effect of pressure increase more directly and more clearly differentiates between the idealized and real jet behavior. This also means that the energetic interpretation of jet behavior provides a more informative basis for understanding pressure-dependent jet performance than a purely kinematic description.
5. The combination of high-speed imaging and motion analysis provided an effective experimental basis for identifying jet dynamics under high-pressure conditions and for assessing the limitations of simplified theoretical models.
6. The obtained results should be treated as a

quantitative basis for further studies on jet development and energy transfer in systems relevant to AWJ applications, particularly in analyses extended to direct interaction with the machined material.

7. The main limitations of the study are related to the simplified character of the analytical model, the estimated character of the acceleration values above 50 MPa, and the fact that direct jet–material interaction was not included in the experimental analysis.

## Acknowledgments

This work/research was supported by NAWA from the STER NAWA Programme within the Project Internationalization of Lublin University of Technology Doctoral School II – IDeaS of LUT II.

## REFERENCES

1. Montesano J, Bougherara H, Fawaz Z. Influence of drilling and abrasive water jet induced damage on the performance of carbon fabric/epoxy plates with holes. Composite Structures. 2017 Mar;163:257–66. https://doi.org/10.1016/j.compstruct.2016.12.007
2. Chen FL, Siores E. The effect of cutting jet variation on striation formation in abrasive water jet cutting. International Journal of Machine Tools and Manufacture. 2001 Aug;41(10):1479–86. https://doi.org/10.1016/S0890-6955(01)00013-X
3. Monno M, Ravasio C. The effect of cutting head vibrations on the surfaces generated by waterjet cutting. International Journal of Machine Tools and Manufacture. 2005 Mar;45(3):355–63. https://doi.org/10.1016/j.ijmachtools.2004.07.010
4. Lemma E, Chen L, Siores E, Wang J. Study of cutting fiber-reinforced composites by using abrasive water-jet with cutting head oscillation. Composite Structures. 2002 Jul;57(1–4):297–303. https://doi.org/10.1016/S0263-8223(02)00097-1
5. Momber AW. The kinetic energy of wear particles generated by abrasive–water-jet erosion. Journal of Materials Processing Technology. 1998 Nov;83(1–3):121–6. https://doi.org/10.1016/S0924-0136(98)00050-8
6. Zelenak M, Foldyna J, Scucka J, Hloch S, Riha Z. Visualisation and measurement of high-speed pulsating and continuous water jets. Measurement. 2015 Aug;72:1–8. https://doi.org/10.1016/j.measurement.2015.04.022
7. Znamenskaya IA, Nersesyan DA, Sysoev NN, Koroteeva EYu, Shirshov YaN. An optical study of high-pressure water-jet dynamics. Moscow Univ Phys. 2016 Jul;71(4):405–12. https://doi.org/10.3103/S0027134916040184
8. Zeleňák M, Říha Z, Jandačka P. Visualization and velocity analysis of a high-speed modulated water jet generated by a hydrodynamic nozzle. Measurement. 2020 Jul;159:107753. https://doi.org/10.1016/j.measurement.2020.107753
9. Li M, Su T, Lin X. Improving surface striation and kerf taper of hybrid Al/CFRP stacks using dual-pass abrasive waterjet slotting strategy. Int J Adv Manuf Technol. 2024 Feb;130(11–12):5763–76. https://doi.org/10.1007/s00170-024-13084-y
10. Du M, Zhang K, Liu Y, Feng L, Fan C. Experimental and simulation study on the influence factors of abrasive water jet machining ductile materials. Energy Reports. 2022 Nov;8:11840–57. https://doi.org/10.1016/j.egyr.2022.09.035
11. Schwartzentruber J, Papini M, Spelt JK. Characterizing and modelling delamination of carbon-fiber epoxy laminates during abrasive waterjet cutting. Composites Part A: Applied Science and Manufacturing. 2018 Sep;112:299–314. https://doi.org/10.1016/j.compositesa.2018.06.014
12. Kartal F. Abrasive water jet machining of carbon fiber-reinforced PLA composites: Optimization of machinability and surface integrity for high-precision applications. Polymers. 2025 Feb 8;17(4):445. https://doi.org/10.3390/polym17040445
13. Hejjaji A, Zitoune R, Crouzeix L, Roux SL, Collombet F. Surface and machining induced damage characterization of abrasive water jet milled carbon/epoxy composite specimens and their impact on tensile behavior. Wear. 2017 Apr;376–377:1356–64. https://doi.org/10.1016/j.wear.2017.02.024
14. Guo LH, Deng SS, Yang X. Numerical simulation of abrasive water jet cutting chemical pipeline based on sph coupled fem. Chemical Engineering Transactions. 2016 Jul;51:73–8. https://doi.org/10.3303/CET1651013
15. Yu R, Hao G, Yang W, Li Z. An unresolved SPH-DEM model for simulation of ductile and brittle surface erosion by abrasive water-jet (AWJ) impact. Sci Rep. 2024 Oct 30;14(1):26115. https://doi.org/10.1038/s41598-024-77009-1
16. Zaki M, Corre C, Kuszla P, Chinesta F. Numerical simulation of the abrasive waterjet (awj) machining: multi-fluid solver validation and material removal model presentation. Int J Mater Form. 2008 Apr;1(S1):1403–6. https://doi.org/10.1007/s12289-008-0127-8
17. Wang J, Gao N, Gong W. Abrasive waterjet machining simulation by SPH method. Int J Adv Manuf Technol. 2010 Sep;50(1–4):227–34. https://doi.org/10.1007/s00170-010-2521-x

18. Ozcan Y, Tunc LT, Kopacka J, Cetin B, Sulitka M. Modelling and simulation of controlled depth abrasive water jet machining (AWJM) for roughing passes of free-form surfaces. Int J Adv Manuf Technol. 2021 Jun;114(11–12):3581–96. https://doi.org/10.1007/s00170-021-07131-1
19. Popan IA, Balc N, Popan AI. Avoiding carbon fibre reinforced polymer delamination during abrasive water jet piercing: a new piercing method. Int J Adv Manuf Technol. 2022 Mar;119(1–2):1139–52. https://doi.org/10.1007/s00170-021-08294-7
20. Vundavilli PR, Parappagoudar MB, Kodali SP, Benguluri S. Fuzzy logic-based expert system for prediction of depth of cut in abrasive water jet machining process. Knowledge-Based Systems. 2012 Mar;27:456–64. https://doi.org/10.1016/j.knosys.2011.10.002
21. Popan IA, Bocăneț VI, Softic S, Popan AI, Panc N, Balc N. Artificial intelligence model used for optimizing abrasive water jet machining parameters to minimize delamination in carbon fiber-reinforced polymer. Applied Sciences. 2024 Sep 21;14(18):8512. https://doi.org/10.3390/app14188512
22. Spadło S, Krajcarz D. Basic abrasive waterjet cutting process parameters. Atest. 2018 Dec 31;19(12):654–7. https://doi.org/10.24136/Atest.2018.472 (in Polish).
23. Qian Y, Cai J, Wan L, Wang X, Wang Z, Chen Y. Experimental study on the kerf characteristic and cross-section quality of CFRP laminates cut by steel slag abrasive waterjet. Int J Adv Manuf Technol. 2025 Mar;137(5–6):2547–62. https://doi.org/10.1007/s00170-025-15297-1
24. Perec A, Kawecka E, Zajac W. AWJ cutting process quality modeling and optimization based on footprint angle. Materials. 2025 Dec 10;18(24):5548. https://doi.org/10.3390/ma18245548
25. Ning D, Wang Q, Tian J, Gong Y, Du H, Chen S, et al. Experimental study on the coating removing characteristics of high-pressure water jet by micro jet flow. Micromachines. 2021 Feb 10;12(2):173. https://doi.org/10.3390/mi12020173
26. Altin Karataş M, Gökkaya H. A review on machinability of carbon fiber reinforced polymer (CFRP) and glass fiber reinforced polymer (GFRP) composite materials. Defence Technology. 2018 Aug;14(4):318–26. https://doi.org/10.1016/j.dt.2018.02.001